AGU ADVANCING EARTH AND SPACE SCIENCE

Geophysical Research Letters

RESEARCH LETTER

10.1029/2023GL104606

Extreme Precipitation-Temperature Scaling in California: The Role of Atmospheric Rivers

Nasser Najibi[1] and Scott Steinschneider[1]

[1]Department of Biological and Environmental Engineering, Cornell University, Ithaca, NY, USA

Key Points:

- Precipitation-temperature (P-T) scaling rates during atmospheric rivers (ARs) are larger than other precipitation events in California
- P-T scaling rates for AR-based events approach the Clausius-Clapeyron rate (7% per °C) when using dew point temperature
- The differences in P-T scaling rates for ARs versus non-ARs are linked to the sensitivity of moisture content and lifting mechanism to warming

Supporting Information:

Supporting Information may be found in the online version of this article.

Correspondence to:

N. Najibi,
nn289@cornell.edu

Citation:

Najibi, N., & Steinschneider, S. (2023). Extreme precipitation-temperature scaling in California: The role of atmospheric rivers. *Geophysical Research Letters*, *50*, e2023GL104606. https://doi.org/10.1029/2023GL104606

Received 17 MAY 2023
Accepted 22 JUN 2023

Abstract

The sensitivity of atmospheric river (AR)-induced precipitation to climate change is primarily driven by increases in atmospheric water vapor with warming. However, the rate at which AR-based precipitation intensifies with warming and whether this rate differs from non-AR events remains uncertain. This work uses multiple statistical models to estimate regional, extreme precipitation-temperature scaling rates in California for AR and non-AR events. Scaling rates are determined using cold-season daily and hourly precipitation, along with multiple temperature variables to assess robustness of the results. We find that regional scaling rates for ARs are consistently larger than non-ARs, especially for hourly event maxima (posterior median scale rates of 5.7% and 2.4% per °C for ARs and non-ARs, respectively). ARs remain near saturated (i.e., high relative humidity) and exhibit more lift and a stronger increase in specific humidity aloft with warming as compared to non-ARs, helping to explain the difference in precipitation-temperature scaling rates.

Plain Language Summary

Atmospheric rivers are long and narrow conveyor belts of water vapor in the sky that transport moisture in the lower atmosphere. They often cause extreme precipitation that can cause flooding along the west coast of the United States. The rate of intensification of atmospheric river-based precipitation with warming is a fundamental scientific question with important implications for adapting civil infrastructure to climate change. This study aims to quantify the relationship between atmospheric river-based extreme precipitation and temperature, and to determine how it differs from other precipitation events. To do so, we utilize multiple statistical methods to quantify cold-season precipitation-temperature scaling rates at weather stations across California. In our analysis, we consider different temperature variables, timescales of data, and ways of accumulating precipitation during events to determine the robustness of our results. Overall, we find that extreme precipitation increases faster with warming during atmospheric rivers compared to other types of events. This difference is linked to the fact that atmospheric rivers exhibit a more direct increase in moisture content and lift with warming. These results suggest that extreme precipitation during atmospheric rivers will increase faster than other events as temperatures rise in the future, which could accelerate damage linked to future flooding events.

1. Introduction

The intensification of extreme precipitation is a major consequence of climate change (Hennessy et al., 1997; Wu et al., 2013), and it is largely due to the increased moisture-holding capacity of the atmosphere with warming (Allan & Soden, 2008; Trenberth et al., 2003). This capacity increases following the Clausius-Clapeyron (C-C) rate of ~6%–7% per °C (Alduchov & Eskridge, 1996), and early work has argued that extreme precipitation would intensify at a similar rate, all else equal (Allen & Ingram, 2002). However, dynamic (circulation-driven) processes can modulate the rate of extreme precipitation intensification (Masson-Delmotte et al., 2021), complicating extreme precipitation–temperature (P-T) scaling rate estimates. Such estimates are critical, as they form the basis for many adaptation frameworks meant to prepare and design natural and built systems for the future impacts of climate change (Donat et al., 2016; Easterling et al., 2000; Held & Soden, 2006; Seager et al., 2010).

There is a rich literature exploring the nuances in apparent P-T scaling relationships, using both observations and model simulations to evaluate the sensitivity of scaling rate estimates to the choice of precipitation quantiles, season, timescale (daily, sub-daily), temperature type (dew point, dry bulb) and timing (concurrent, antecedent), weather patterns, rainfall type (convective, stratiform), and statistical modeling approach (Lenderink & Van Meijgaard, 2008; O'Gorman & Schneider, 2009a,2009b; Lenderink et al., 2011; Shaw et al., 2011; Panthou et al., 2014; Loriaux et al., 2013; Zhang et al., 2017; Zhang et al., 2019; Magan et al., 2020; Martinkova &

Kysely, 2020; Lenderink et al., 2021; Bello et al., 2021; Fowler et al., 2021; Hosseini-Moghari et al., 2022; Steinschneider & Najibi, 2022). Almost all these studies investigate if and why the derived P-T scaling rates follow, exceed, or fall below the C-C rate. For instance, Ali et al. (2018, 2021) showed that daily P-T scaling rates approximately follow the C-C rate in most locations globally. However, sub-daily rates exceed the C-C rate in some locations (Ali & Mishra, 2017; Ban et al., 2015; Barbero et al., 2018; Drobinski et al., 2018), possibly due to dynamical feedbacks with additional latent heat release from wetter storms (e.g., Lenderink et al., 2021; Lenderink & Van Meijgaard, 2008). More generally, there is a substantial degree of uncertainty in estimated scaling rates (Ali et al., 2022; Najibi et al., 2022; Sun & Wang, 2022; Visser et al., 2020, 2021), which is not always quantified. Consequently, P-T scaling rates remain heavily debated (Fowler et al., 2021; Pendergrass, 2018).

In California, a growing body of work underscores the substantial increase in climate risk due to intensifying extreme precipitation (Cayan et al., 2008; Dettinger et al., 2011; Swain et al., 2018). These events are primarily caused by atmospheric rivers (ARs), which have become more frequent, wetter, and larger in recent decades, and are projected to continue this trend under further warming (Dettinger, 2011; Espinoza et al., 2018; Gao et al., 2015; Gershunov et al., 2019; Groisman et al., 2005; Hagos et al., 2016; Huang et al., 2020; Mahoney et al., 2018; Michaelis et al., 2022; Polade et al., 2017; Rhoades et al., 2020; Shields & Kiehl, 2016; Zhang et al., 2021). Given their importance to present and future flood risk and water supply (Corringham et al., 2019; Dettinger, 2011; Hanak & Lund, 2012; Ralph et al., 2019; Rutz et al., 2014), it is critical to understand the processes that underscore P-T scaling associated with AR-induced heavy precipitation events (Payne et al., 2020).

Several studies have explored these processes using climate models. For instance, Warner et al. (2015) found that GCMs project that the mean AR-related winter precipitation and precipitation on extreme vertically integrated horizontal vapor transport (IVT) days along the U.S. west coast increase respectively by 4%–6% and 5%–19% per °C by the end of the 21st century. Chen and Leung (2020) identified a 3% per °C increase in AR-related precipitation in two regional climate simulations, while Michaelis et al. (2022) showed that total event precipitation associated with two ARs during the Oroville Dam crisis of 2017 would increase between 11% and 17% per °C under late 21st century warming, with a ~9% per °C increase in precipitable water and additional intensification due to higher IVT linked to stronger winds.

However, surprisingly little work has directly investigated observed (i.e., gauge-based) P-T scaling rates associated with ARs and how they may differ from non-AR events. Several studies have explored apparent scaling rates in observations over California (Prein et al., 2017; Utsumi et al., 2011), but to our knowledge, none have separately estimated scaling rates based on whether precipitation is AR- or non-AR-driven. If such differences in scaling rate exist, they would have important implications for climate change adaptation strategies in regions like California, where ARs have an outsized influence on flood risk. Accurate P-T scaling rate estimates for AR events in particular will be important for adapting flood risk reduction infrastructure to the effects of warming. As others have shown (Berg & Haerter, 2013; Haerter & Berg, 2009), P-T scaling rates can differ across weather systems, and inaccurate rate estimates can result if the data are not first separated by storm type.

We hypothesize that P-T scaling rates will be larger for AR versus non-AR storms, primarily because ARs are near saturated and additional atmospheric moisture with warming will precipitate out with orographic lift (Algarra et al., 2020; Lundquist et al., 2010; B. L. Smith et al., 2010). The processes driving non-AR precipitation are more dynamic and complex, which could lower apparent P-T scaling rates by weakening the relationship between temperature, additional atmospheric moisture, saturation level, and extreme precipitation. To test this hypothesis, this work uses daily and hourly records of precipitation and temperature to compare regional P-T scaling rates associated with AR and non-AR precipitation events in California. We utilize multiple statistical modeling frameworks, including a novel, Bayesian regression model, to quantify regional P-T scaling rates with uncertainty, and evaluate the sensitivity of our inferred scaling rates to different modeling choices to assess the robustness of our results. We also examine differences in the response of humidity and lift to warming for AR and non-AR events to identify the key factors that explain scaling rate differences that emerge between the two storm types.

2. Data and Methods

2.1. Precipitation, Dry-Bulb Temperature, and Dew Point Temperature

We obtained daily and hourly observations of precipitation (P, mm), dry-bulb temperature (Ta, °C), and dew point temperature (Td, °C) at the near-surface (2 m) from the Global Summary of the Day and Global Hourly

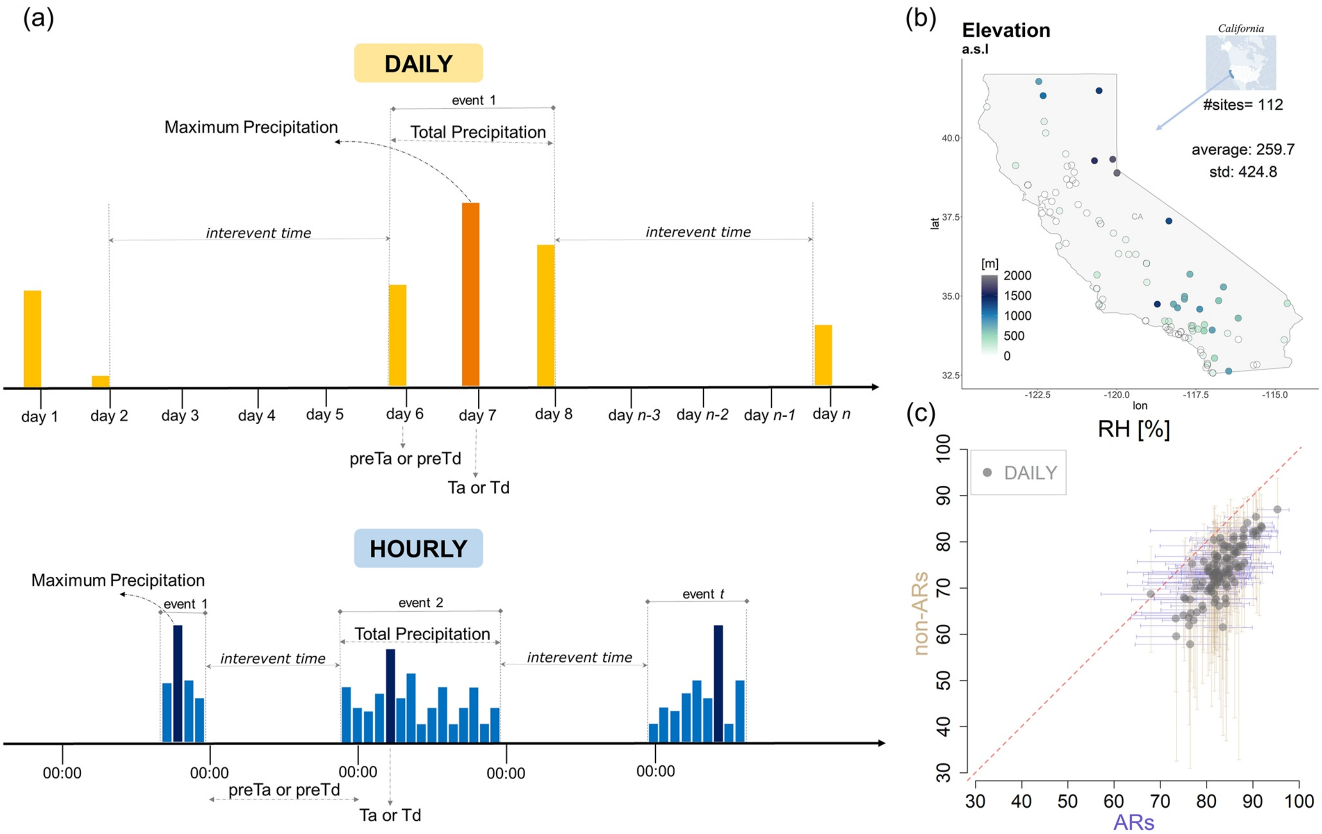

Figure 1. (a) Definition of total and maximum precipitation events with a 3-day and 24-hr interevent interval at daily (top) and hourly (bottom) timescales, along with associated temperature variables. Average precipitation is also defined as the mean of total precipitation only during the rainy days or hours. (b) Location of 112 co-located daily and hourly weather stations with their elevation above sea level (a.s.l). (c) Daily relative humidity (RH, in %) at 850 hPa for precipitation events associated and not associated with atmospheric rivers (ARs). Points represent the median RH for different weather stations across the entire set of events under each AR category, and the whiskers indicate the 25th and 75th percentiles of RH across all events.

datasets within the Integrated Surface Database (ISD; A. Smith et al., 2011). We identified all daily sites across California with a minimum of 330 days of non-missing data for P, Ta, and Td in each year and at least 10 years of record between 01 January 1948, and 31 December 2021. We also compiled hourly sites that are co-located with the daily sites, requiring a yearly minimum of 30 days and at least 5 years of data. This resulted in 112 sites with daily and hourly records that had over 25 and 18 years of data on average per site, respectively (Figure 1b). We only retained daily and hourly observations during the cold-season (November-April) that passed quality control checks in the ISD (i.e., code "1") for all three variables (P, Ta, and Td), and all trace precipitation records were discarded (Lott et al., 2001).

We also obtained hourly 850 hPa Ta, relative humidity (RH, %), specific humidity (SH, kg/kg), and vertical velocity (Omega, Pa/s) from the European Centre for Medium-Range Weather Forecasts (ECMWF) ERA5 reanalysis (0.25° resolution) from 1979 to 2021 (Hersbach et al., 2020). These data are used to help estimate temperature, humidity, and lifting mechanisms in the lower atmospheric column where most of the AR moisture is present (Ralph et al., 2004, 2005; B. L. Smith et al., 2010). Hourly values were averaged to the daily timestep, and Td was calculated using Ta and RH following Anderson et al. (2016). The reanalysis data was associated with each ISD station by averaging data from the four grid cells nearest to each station.

2.2. Archives of AR-Induced Precipitation in California

We used the Scripps Institution of Oceanography (SIO)-generated catalog of ARs landfalls (SIO-R1 catalog) along the west coast of North America (20–60°N) during 1948–2015 (Gershunov et al., 2017) to separate AR and non-AR precipitation events across California. Gershunov et al. (2017) produced a 0.0625° (~6 km) daily gridded

10.1029/2023GL104606

precipitation product based on the precipitation data in Livneh et al. (2013) that flags each precipitation value as associated or not associated with ARs. For each of our meteorological stations from Section 2.1, we tagged the daily or hourly data in each site as AR-related if at least one of the eight closest grid cells in the gridded precipitation product from Gershunov et al. (2017) was tagged as being AR driven.

2.3. Precipitation Events

We define a precipitation event as a block of time during which one or more precipitation bursts greater than trace precipitation occur in close succession, possibly with a short intermediate period of zero or trace precipitation (e.g., Bello et al., 2022; Visser et al., 2021; Wasko et al., 2015). We clustered daily and hourly P into events by requiring a 3-day and 24-hr minimum interval of dry conditions (i.e., trace precipitation or less) between separate events, respectively (Figure 1a). For each event, we then defined maximum event P as the peak value of daily or hourly precipitation within the event, and average event P as the mean of daily or hourly non-zero precipitation values during the event duration. We select average event P instead of total event P because we found that longer duration events generally had greater total P and were warmer, which could artificially inflate scaling rate estimates. This effect of event duration is removed by using average event P.

We also defined several temperature values for each precipitation event. Concurrent Ta and Td were defined as the temperatures occurring at the time of maximum daily or hourly precipitation, while preceding temperatures (preTa, preTd) were defined as the Ta and Td occurring 1 day prior to the maximum daily or hourly precipitation. Note that average hourly temperatures for the entire day prior to maximum P were used to define preTa and preTd for hourly events. This procedure was applied to both Ta and Td at the surface (station-based) and 850 hPa (reanalysis based). Ultimately, for both daily and hourly events, we defined two precipitation variables (average precipitation, maximum precipitation) at the surface, and eight temperature variables (Ta, Td, preTa, and preTd at the surface and 850 hPa).

2.4. Models to Estimate Precipitation-Temperature Scaling Relationships

We utilize multiple models to estimate P-T scaling rates in order to assess the sensitivity of our results to the choice of statistical method and temperature variable.

2.4.1. Hierarchical Bayesian Quantile Regression

Our primary model follows the approach of Najibi et al. (2022), which uses a hierarchical Bayesian quantile regression model to quantify both at-site and regional P-T scaling rates for a high precipitation quantile ($q = 0.99$), conditioned on AR and non-AR precipitation events. Two layers are embedded within the hierarchical model, whereby log-transformed P is regressed on temperature in the first layer, while regression coefficients vary based on the occurrence of ARs or non-ARs in the second layer. The model for site i, event t, and non-AR/AR occurrence $k \in \{0, 1\}$ is formulated as follows:

Layer I. Precipitation–Temperature Scaling

$$
\begin{gathered}
ln(\boldsymbol{P}_{i,t}) \sim \mathrm{Normal}\left(\mu_{p_{i,t}}{}', \sigma^2_{p_{i,t}}{}'\right) \\
\mu_{p_{i,t}}{}' = \frac{1-2q}{q(1-q)} w_{i,t} + \mu_{p_{i,t}} \\
\mu_{p_{i,t}} = \alpha_{i,k(t)} + \beta_{i,k(t)} \boldsymbol{T}_{i,t} \\
\sigma^2_{p_{i,t}}{}' = \frac{2 w_{i,t}}{\upsilon_i q(1-q)} \\
\upsilon_i \sim \mathrm{Uniform}(0, 100);\ w_{i,t} \sim \mathrm{Exponential}(\upsilon_i)
\end{gathered} \tag{1}
$$

Layer II. Scaling Rate by AR State

$$
\alpha_{i,k(t)} \sim \mathrm{Normal}(0, 100)
$$

$$
\beta_{i,k(t)} \sim \mathrm{Normal}\left(\mu_k, \sigma_k^2\right)
$$

$$\mu_k \sim \mathrm{Normal}(0,1);\ \sigma_k \sim \mathrm{InverseGamma}(1,10) \tag{2}$$

The model is a Bayesian version (Yu & Moyeed, 2001) of the quantile regression approach used in Wasko and Sharma (2014), with a likelihood function modeled using a scale mixture of normal distributions, an exponential random deviate $w_{i,t}$ with rate v_i that varies by site i, and a skewness parameter corresponding to the precipitation quantile (q). Readers are directed to Najibi et al. (2022) for additional detail on the model structure.

The coefficients $\alpha_{i,k(t)}$ and $\beta_{i,k(t)}$ in Layer I vary in time depending on whether the precipitation event t is associated with an AR ($k(t) = 1$) or non-AR ($k(t) = 0$). In Layer II, the intercepts $\alpha_{i,k(t)}$ are given vague priors independently for each site and AR state. The coefficients $\beta_{i,k(t)}$ that determine how precipitation scales with temperature are partially pooled across sites via a normal distribution. This distribution has hyperparameters μ_k and σ_k that define a regional average and standard deviation of P-T scaling based on AR and non-AR occurrence. Not only does the partial pooling help to stabilize parameter estimation across sites, but inference on the posterior distribution of μ_k for $k = 0$ and $k = 1$ provides a direct measure of whether P-T scaling rates at a regional scale differ based on whether or not precipitation events are associated with ARs. The coefficient μ_k can be expressed as a percent change per °C warming using $(e^{\mu_k} - 1) \times 100\%$.

2.4.2. Other Scaling Rate Estimation Models

To assess the sensitivity of our results to the choice of statistical method, we also evaluated scaling rates estimated on a site-by-site basis using non-parametric binning, quantile regression, and trend scaling models (e.g., Ali et al., 2018; Lenderink & Van Meijgaard, 2010; Loriaux et al., 2013; Wasko & Sharma, 2014; Zhang et al., 2017). We note that these approaches, while more common in the literature, tend to be noisier due to a lack of spatial information pooling and provide less rigorous uncertainty quantification. Finally, we also employ a hierarchical Bayesian version of trend scaling regression (Zhang et al., 2017) that differs from the quantile regression in Section 2.4.1 by focusing specifically on the most extreme precipitation events. This approach is described in more detail in Text S1 in Supporting Information S1.

2.4.3. Application and Estimation

All models above are estimated separately using (a) daily and hourly datasets; (b) average and maximum event precipitation; and (c) eight temperature variables (Ta, Td, preTa, and preTd at the surface and 850 hPa). Overall, 32 different models are estimated for each statistical method, enabling a thorough sensitivity analysis of the inferred scaling rates to modeling choices. However, we focus our attention on a subset of results that use the most physically consistent set of variables based on past literature, namely: concurrent gauge-based dew point temperatures for daily events (dew point temperatures to better represent moisture availability; Ali et al., 2018), and antecedent gauge-based dew point temperatures for hourly events (antecedent temperatures to address the effects of short-term atmospheric cooling; Visser et al., 2020). Since P-T scaling rate estimates are sensitive to small sample sizes, a minimum of 150 and 30 events per site were required for a site to be included in the quantile regression and trend scaling models, respectively. Figure S1 in Supporting Information S1 shows the distribution of events per site under each combination of variables from different datasets.

Parameters for all Bayesian models were estimated using JAGS (Denwood, 2016; Plummer, 2003), using 8,000 iterations across four chains with the last 1,000 iterations kept for inference. We checked for convergence using the Gelman and Rubin criterion (Gelman & Rubin, 1992). To evaluate the statistical significance of scaling rate differences between levels of a factor (e.g., differences in scaling rates between ARs and non-ARs), we calculate the percentage of posterior samples for which scaling rate differences across levels of that factor are greater than or less than zero. We require 95% of posterior differences to be all above or below zero for the differences to be considered significant.

3. Results

3.1. Scaling Rate Estimates

Figure 2a shows the regional P-T scaling rates computed based on the hierarchical Bayesian quantile regression method of Section 2.4.1. We present the posterior distribution of regional scaling rates (μ_k) for the 99th percentile of precipitation with Td (daily) and preTd (hourly) at the surface. Statistical significance across the full suite of 32 different model formulations is shown in Figure S2 in Supporting Information S1, while results for other temperature variables are shown in Figure S3 in Supporting Information S1.

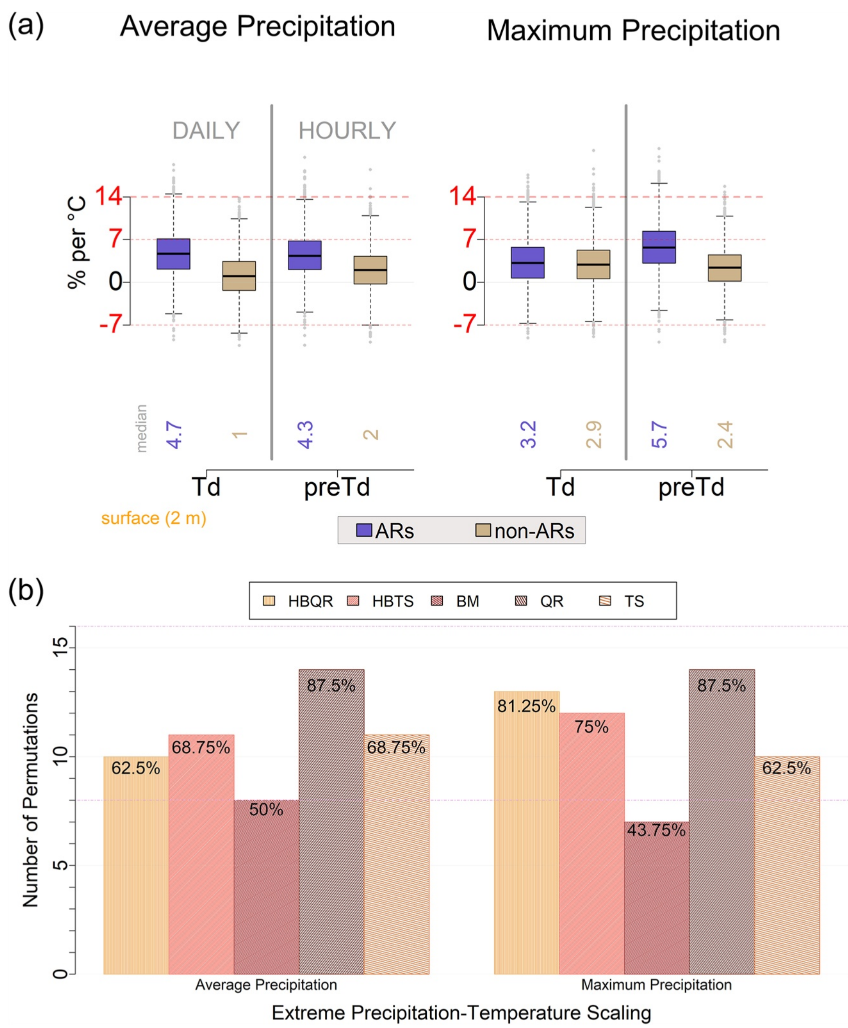

Figure 2. (a) Posterior distribution of regional P-T scaling rates (μ) based on the hierarchical Bayesian quantile regression, separated for AR- and non-AR events. Results shown for average event precipitation (left) and maximum event precipitation (right) at hourly and daily timescales and for the 99th percentile, based on dew point temperature (Td) and preceding Td (preTd) at the surface. (b) Number (and %) of model formulations where median P-T scaling rates for AR events exceed non-AR events, shown for different methods including hierarchical Bayesian quantile regression (HBQR), hierarchical Bayesian trend scaling (HBTS), at-site binning method (BM), at-site quantile regression (QR), and at-site trend scaling (TS). Regional estimates are shown for HBQR and HBTS, while the median of at-site estimates are shown for BM, QR, and TS. There are 16 model permutations for average precipitation (left) and maximum precipitation (right), including four temperatures (Ta, Td, preTa, preTd), two levels (surface, 850 hPa), and two timescales (daily, hourly).

Figure 2a shows that scaling rates for ARs are larger than non-ARs for both average and maximum event precipitation at both daily and hourly timescales. These differences are statistically significant at the 95% level. The largest median scaling rate for non-ARs in Figure 2a is 2.9% per °C (hourly maximum precipitation with Td), while the largest median scaling rate for ARs is 5.7% per °C (hourly maximum precipitation with preTd). Figure S2 in Supporting Information S1 shows that in total, 21 (23) of the 32 different models show posterior scaling rates that are significantly larger under ARs versus non-ARs at the 95% (90%) level. In only 6 instances are posterior scaling rates significantly larger under non-AR events at the 95% level, and in all these cases temperatures are based on Ta or preTa rather than Td or preTd. In 3 instances, the distributions of regional scaling rates are not statistically distinguishable between storm type. It is important to note that despite the significant differences in regional scaling rates between ARs and non-ARs, the uncertainty in scaling rates for any one formulation remains large. For example, while the median regional scaling rate for ARs is 5.7% per °C when using hourly maximum precipitation and preTd, the interquartile range spans from 3.1% to 8.4% per °C.

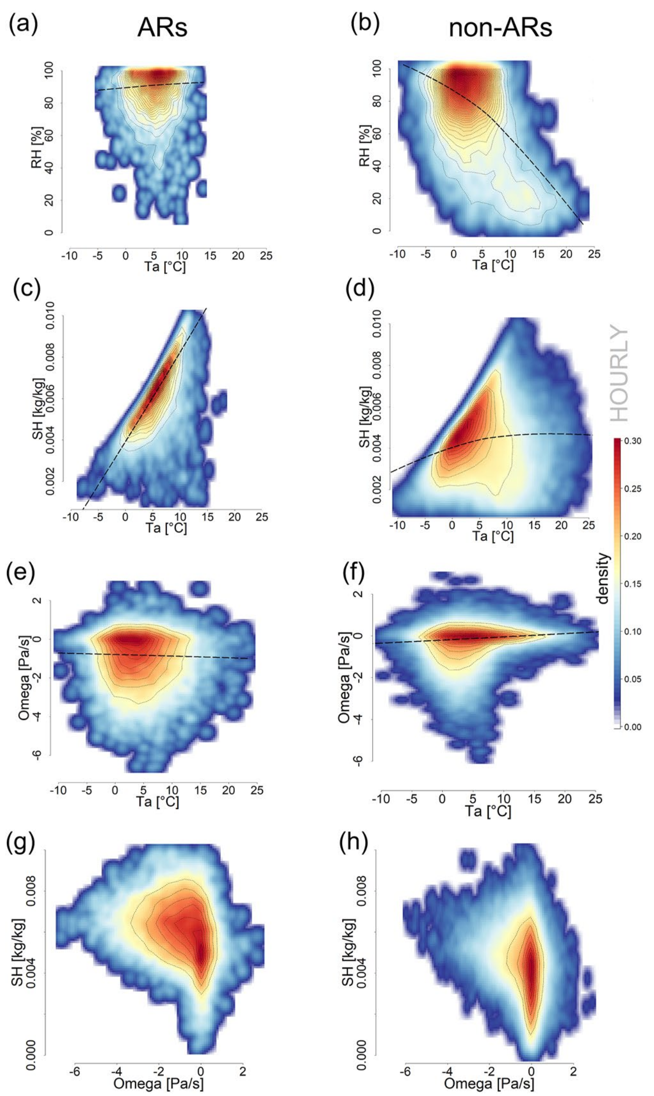

Figure 3. Changes in relative humidity (RH) (a, b), specific humidity (SH) (c, d), and vertical velocity (Omega) (e, f) with dry-bulb temperature (Ta) and SH with Omega (g, h) at 850 hPa for hourly precipitation events conditioned on ARs (left) and non-ARs (right). A locally weighted scatterplot smoothing is drawn as a black long-dashed line in Ta plots.

Two other notable results also arise from the full suite of 32 different model formulations (Figures S2 and S3 in Supporting Information S1). First, the choice of dew point temperature or dry bulb temperature explains the most variation (15% and 5% for ARs and non-ARs, respectively) across scaling rate estimates, based on an ANOVA applied to all posterior samples pooled across temperature factors (dry bulb vs. dew point, surface vs. 850 hPa, antecedent vs. concurrent). With only a few exceptions, the scaling rates are greater for Td versus Ta and preTd versus preTa, consistent with previous work finding that dew point temperature provides a better measure of moisture availability for scaling rate estimation (e.g., Ali et al., 2018; Barbero et al., 2018; Wasko et al., 2018). Second, for hourly data preTd consistently leads to higher scaling rates than concurrent Td for both event averages and event maxima, at both atmospheric temperature levels, and for both storm types. This is consistent with previous work showing that antecedent temperatures can better address the effects of short-term atmospheric cooling on scaling rate estimation (Visser et al., 2020). This effect is not seen consistently for daily data, where the signal is more mixed across storm types and event averages versus maxima.

To further evaluate the sensitivity of our results to modeling choice, we also estimate P-T scaling rates for all 32 formulations via the binning method (Figure S4 in Supporting Information S1), standard quantile regression (Figure S5 in Supporting Information S1), trend scaling (Figure S6 in Supporting Information S1), and a hierarchical Bayesian version of the trend scaling model (Figures S7 and S8 in Supporting Information S1) (see Section 2.4.2). The non-Bayesian models are applied site-by-site, the median scaling rate is taken across all 112 sites, and then these medians are compared for AR and non-AR events. Posterior median regional scaling rates between ARs and non-ARs are compared directly for the hierarchical Bayesian trend scaling model (Text S1 in Supporting Information S1). We synthesize results from all models in Figure 2b, counting the number of formulations in which median scaling rates for ARs are larger than non-ARs. We separate the results for event averages and event maxima. There is a clear pattern by which ARs exhibit higher P-T scaling rates than non-ARs for both event averages and maxima. The only exception is the binning method, for which neither storm type exhibits consistently higher scaling rates. We should note though that the binning approach can result in bias in scaling rate estimates due to uneven sample sizes across temperature bins, particularly for bins associated with the warmest or coldest temperatures (Wasko & Sharma, 2014).

3.2. Physical Mechanisms Behind Scaling Rate Differences Between ARs and Non-ARs

To better understand the reason why P-T scaling rates differ between ARs and non-ARs, we examine the changes in atmospheric moisture content and lift with warming under each storm type. We use a 2D density plot (Figure 3) to show how RH, SH, and Omega vary with Ta, and how SH varies with Omega, all based on ERA5 at 850 hPa. Results are shown for all hourly precipitation events associated with ARs (Figures 3a, 3c, 3e, and 3g) and non-ARs (Figures 3b, 3d and 3f, 3h) across all sites. We note that results also hold true when only applied to more extreme hourly events, that is, only events with maximum precipitation greater than the site-specific 90th percentile of non-zero precipitation (Figure S9 in Supporting Information S1).

For ARs, RH remains consistent and high when Ta rises because of the monotonic increase in SH with warming (Figure 3a). That is, as ARs warm, they remain saturated and increase in their water vapor content. A similar pattern is not seen as clearly for non-ARs (Figure 3b). For these storms, SH does not increase with Ta (Figure 3d) as consistently as it does for ARs (Figure 3c), and consequently, RH has a tendency to decline with warming (Figure 3b). In Figures 3e and 3f, a slightly upsloping line and tight scatter for non-ARs indicates that warm non-ARs never get the large lift, but that is not the case for the ARs, as warm ARs still get significant lift (Figure 3e). We also find that ARs more frequently exhibit greater uplift than non-ARs, especially at high levels of specific humidity (see Figures 3g and 3h).

These results are consistent with the higher P-T scaling rates found for AR events compared to non-AR events. During ARs, warming is linked to a direct increase in atmospheric water content in an already near-saturated environment. In conjunction with enhanced uplift during these warm events, much of this added moisture leads to intensifying precipitation as temperatures warm. In non-AR environments, the response to warming is more subdued. Atmospheric moisture content does increase with warming, but not as consistently as ARs. Therefore, as the moisture holding capacity of the atmosphere increases with higher temperatures, there is a tendency for RH to decline during non-AR events. Coupled with weaker uplift, this leads to a slower rate of precipitation increase with warmer temperatures. Additional analysis suggests that the decrease in RH with warming during non-AR events is associated with different large-scale circulation patterns during warm and cold non-AR events. Specifically, warm (>10°C) and cold (<10°C) non-AR events are commonly associated with high- and low-pressure systems over the Western US, while ARs generally exhibit the same large-scale circulation independent of temperature (Figure S10 in Supporting Information S1). During warm non-AR events, descending air under the anomalous high warms the air through adiabatic heating, while moisture converge is suppressed. Consequently, the moisture holding capacity of the air increases without coincident increases in atmospheric moisture, resulting in relatively flat SH and declining RH with warming.

4. Conclusions

This study contributes a novel comparison of P-T scaling rates estimated across California, with a specific focus on differences in scaling rates between AR and non-AR events. We employ a hierarchical Bayesian model to support the estimation of regional scaling rates with uncertainty, and test the sensitivity of our results to choice of timescale, temperature variable, precipitation event metric, and statistic model using additional 4 models and 32 separate formulations. The two primary conclusions of this study are as follows:

- Extreme precipitation associated with ARs consistently scales with temperature at a higher rate than non-AR precipitation. These results are robust across multiple models, temperature variables, and for both event-based precipitation averages and maxima, but are especially apparent when scaling rates are based on dew point temperature.
- The differences in P-T scaling rates between AR and non-AR events are associated with greater increases in moisture content with warming, a stronger lifting mechanism, and stable levels of saturation within AR storm systems. Moisture content in non-AR systems grows more slowly with warming and saturation levels decline, leading to lower P-T scaling rates.

On average, ARs have higher relative humidity, are warmer, and lead to more precipitation compared to non-AR storms (see Figure 1c; Figures S11–S14 in Supporting Information S1). Therefore, any increases in atmospheric moisture content due to additional warming will more directly result in greater precipitation, especially for larger events that are already saturated and exhibit substantial uplift (Figure 3). This is consistent with previous research (Wang & Sun, 2022) and a growing consensus that increases in AR-based atmospheric moisture with warming will drive more intense precipitation events, especially in regions with elevated terrain like California (e.g., Payne et al., 2020). Conversely, the environments driving non-AR extreme precipitation are more complex and less clearly driven by changes in atmospheric moisture content (Rhoades et al., 2020).

We recognize that the P-T scaling rate estimates in this study are derived from historical meteorology, and it is possible that future extreme events stemming from ARs with different characteristics (e.g., stronger winds) could exhibit different scaling behavior (e.g., Gao et al., 2015; Michaelis et al., 2022; Zhang et al., 2021). In addition, more investigation is needed to isolate the relationship between extreme AR precipitation intensification and warming of background temperatures on land, along the AR track, and over local and remote ocean waters (Algarra et al., 2020; Chen & Leung, 2020; Gonzales et al., 2019; Nusbaumer & Noone, 2018).

Nevertheless, the results presented here demonstrate that ARs should be considered separately from non-ARs when assessing how extreme precipitation changes in the future under warming. This will help to better quantify the risk of future extreme events and tailor adaptation strategies to address them.

Data Availability Statement

The data used in this analysis are publicly available through the NOAA online repository of the Integrated Surface Database (ISD) (https://www.ncei.noaa.gov/products/land-based-station/integrated-surface-database) for daily and hourly precipitation, dry-bulb and dew point temperatures (A. Smith et al., 2011). The ERA5 hourly data on pressure levels are available from the Copernicus Climate Change Service, Climate Data Store (https://doi.org/10.24381/cds.bd0915c6) for dry-bulb temperature, relative humidity, specific humidity, and vertical velocity at 850-hPa level (Hersbach et al., 2020). The SIO-R1 catalog can be accessed at http://cw3e.ucsd.edu/Publications/SIO-R1-Catalog/ (Gershunov et al., 2017). The codes relevant to this paper (Bayesian models) and for replicating the results can be accessed through the GitHub (https://github.com/nassernajibi/extreme-precipitation-temperature-scaling-in-California) and Zenodo permanent repository at https://doi.org/10.5281/zenodo.7390670 (Najibi, 2023).

Acknowledgments

This work was supported by the California Department of Water Resources and Turlock Irrigation District. We thank Alexander Gershunov, Tamara Shulgina, and Alexander Weyant for providing access to the SIO-R1 catalog and feedback on this analysis.

References

Alduchov, O. A., & Eskridge, R. E. (1996). Improved Magnus form approximation of saturation vapor pressure. *Journal of Applied Meteorology and Climatology*, *35*(4), 601–609. https://doi.org/10.1175/1520-0450(1996)035<0601:imfaos>2.0.co;2

Algarra, I., Nieto, R., Ramos, A. M., Eiras-Barca, J., Trigo, R. M., & Gimeno, L. (2020). Significant increase of global anomalous moisture uptake feeding landfalling Atmospheric Rivers. *Nature Communications*, *11*(1), 1–7. https://doi.org/10.1038/s41467-020-18876-w

Ali, H., Fowler, H. J., Lenderink, G., Lewis, E., & Pritchard, D. (2021). Consistent large-scale response of hourly extreme precipitation to temperature variation over land. *Geophysical Research Letters*, *48*(4), e2020GL090317. https://doi.org/10.1029/2020gl090317

Ali, H., Fowler, H. J., & Mishra, V. (2018). Global observational evidence of strong linkage between dew point temperature and precipitation extremes. *Geophysical Research Letters*, *45*(22), 12320–12330. https://doi.org/10.1029/2018gl080557

Ali, H., Fowler, H. J., Pritchard, D., Lenderink, G., Blenkinsop, S., & Lewis, E. (2022). Towards quantifying the uncertainty in estimating observed scaling rates. *Geophysical Research Letters*, *49*(12), e2022GL099138. https://doi.org/10.1029/2022gl099138

Ali, H., & Mishra, V. (2017). Contrasting response of rainfall extremes to increase in surface air and dewpoint temperatures at urban locations in India. *Scientific Reports*, *7*(1), 1–15. https://doi.org/10.1038/s41598-017-01306-1

Allan, R. P., & Soden, B. J. (2008). Atmospheric warming and the amplification of precipitation extremes. *Science*, *321*(5895), 1481–1484. https://doi.org/10.1126/science.1160787

Allen, M. R., & Ingram, W. J. (2002). Constraints on future changes in climate and the hydrologic cycle. *Nature*, *419*(6903), 228–232. https://doi.org/10.1038/nature01092

Anderson, G. B., Peng, R. D., & Ferreri, J. M. (2016). *weathermetrics: Functions to convert between weather metrics*. National Weather Service Hydrometeorological Prediction Center Web Team.

Ban, N., Schmidli, J., & Schär, C. (2015). Heavy precipitation in a changing climate: Does short-term summer precipitation increase faster? *Geophysical Research Letters*, *42*(4), 1165–1172. https://doi.org/10.1002/2014gl062588

Barbero, R., Westra, S., Lenderink, G., & Fowler, H. J. (2018). Temperature-extreme precipitation scaling: A two-way causality? *International Journal of Climatology*, *38*(S1), e1274–e1279. https://doi.org/10.1002/joc.5370

Bello, A. P., Mailhot, A., & Paquin, D. (2021). The response of daily and sub-daily extreme precipitations to changes in surface and dew-point temperatures. *Journal of Geophysical Research: Atmospheres*, *126*(16), e2021JD034972. https://doi.org/10.1029/2021JD034972

Bello, A. P., Mailhot, A., Paquin, D., & Paquin-Ricard, D. (2022). Temperature-precipitation scaling rates: A rainfall event-based perspective. *Journal of Geophysical Research: Atmospheres*, *127*, e2022JD037873. https://doi.org/10.1029/2022JD037873

Berg, P., & Haerter, J. O. (2013). Unexpected increase in precipitation intensity with temperature — A result of mixing of precipitation types? *Atmospheric Research*, *119*, 56–61. https://doi.org/10.1016/j.atmosres.2011.05.012

Cayan, D. R., Maurer, E. P., Dettinger, M. D., Tyree, M., & Hayhoe, K. (2008). Climate change scenarios for the California region. *Climatic Change*, *87*(1), 21–42. https://doi.org/10.1007/s10584-007-9377-6

Chen, X., & Leung, L. R. (2020). Response of landfalling atmospheric rivers on the US West Coast to local sea surface temperature perturbations. *Geophysical Research Letters*, *47*(18), e2020GL089254. https://doi.org/10.1029/2020gl089254

Corringham, T. W., Ralph, F. M., Gershunov, A., Cayan, D. R., & Talbot, C. A. (2019). Atmospheric rivers drive flood damages in the western United States. *Science Advances*, *5*(12), eaax4631. https://doi.org/10.1126/sciadv.aax4631

Denwood, M. J. (2016). Runjags: An R package providing interface utilities, model templates, parallel computing methods and additional distributions for MCMC models in JAGS. *Journal of Statistical Software*, *71*(9), 1–25. https://doi.org/10.18637/jss.v071.i09

Dettinger, M. (2011). Climate change, atmospheric rivers, and floods in California–a multimodel analysis of storm frequency and magnitude changes. *JAWRA Journal of the American Water Resources Association*, *47*(3), 514–523. https://doi.org/10.1111/j.1752-1688.2011.00546.x

Dettinger, M. D., Ralph, F. M., Das, T., Neiman, P. J., & Cayan, D. R. (2011). Atmospheric rivers, floods and the water resources of California. *Water*, *3*(2), 445–478. https://doi.org/10.3390/w3020445

Donat, M. G., Lowry, A. L., Alexander, L. V., O'Gorman, P. A., & Maher, N. (2016). More extreme precipitation in the world's dry and wet regions. *Nature Climate Change*, *6*(5), 508–513. https://doi.org/10.1038/nclimate2941

Drobinski, P., Silva, N. D., Panthou, G., Bastin, S., Muller, C., Ahrens, B., et al. (2018). Scaling precipitation extremes with temperature in the Mediterranean: Past climate assessment and projection in anthropogenic scenarios. *Climate Dynamics*, *51*(3), 1237–1257. https://doi.org/10.1007/s00382-016-3083-x

Easterling, D. R., Meehl, G. A., Parmesan, C., Changnon, S. A., Karl, T. R., & Mearns, L. O. (2000). Climate extremes: Observations, modeling, and impacts. *Science*, *289*(5487), 2068–2074. https://doi.org/10.1126/science.289.5487.2068

Espinoza, V., Waliser, D. E., Guan, B., Lavers, D. A., & Ralph, F. M. (2018). Global analysis of climate change projection effects on atmospheric rivers. *Geophysical Research Letters*, *45*(9), 4299–4308. https://doi.org/10.1029/2017gl076968

Fowler, H. J., Lenderink, G., Prein, A. F., Westra, S., Allan, R. P., Ban, N., et al. (2021). Anthropogenic intensification of short-duration rainfall extremes. *Nature Reviews Earth & Environment*, *2*(2), 107–122. https://doi.org/10.1038/s43017-020-00128-6

Gao, Y., Lu, J., Leung, L. R., Yang, Q., Hagos, S., & Qian, Y. (2015). Dynamical and thermodynamical modulations on future changes of landfalling atmospheric rivers over western North America. *Geophysical Research Letters*, *42*(17), 7179–7186. https://doi.org/10.1002/2015gl065435

Gelman, A., & Rubin, D. B. (1992). Inference from iterative simulation using multiple sequences. *Statistical Science*, *7*(4), 457–472. https://doi.org/10.1214/ss/1177011136

Gershunov, A., Shulgina, T., Clemesha, R. E., Guirguis, K., Pierce, D. W., Dettinger, M. D., et al. (2019). Precipitation regime change in Western North America: The role of atmospheric rivers. *Scientific Reports*, *9*(1), 1–11. https://doi.org/10.1038/s41598-019-46169-w

Gershunov, A., Shulgina, T., Ralph, F. M., Lavers, D. A., & Rutz, J. J. (2017). Assessing the climate-scale variability of atmospheric rivers affecting western North America. *Geophysical Research Letters*, *44*(15), 7900–7908. https://doi.org/10.1002/2017gl074175

Gonzales, K. R., Swain, D. L., Nardi, K. M., Barnes, E. A., & Diffenbaugh, N. S. (2019). Recent warming of landfalling atmospheric rivers along the west coast of the United States. *Journal of Geophysical Research: Atmospheres*, *124*(13), 6810–6826. https://doi.org/10.1029/2018jd029860

Groisman, P. Y., Knight, R. W., Easterling, D. R., Karl, T. R., Hegerl, G. C., & Razuvaev, V. N. (2005). Trends in intense precipitation in the climate record. *Journal of Climate*, *18*(9), 1326–1350. https://doi.org/10.1175/jcli3339.1

Haerter, J. O., & Berg, P. (2009). Unexpected rise in extreme precipitation caused by a shift in rain type? *Nature Geoscience*, *2*(6), 372–373. https://doi.org/10.1038/ngeo523

Hagos, S. M., Leung, L. R., Yoon, J. H., Lu, J., & Gao, Y. (2016). A projection of changes in landfalling atmospheric river frequency and extreme precipitation over western North America from the Large Ensemble CESM simulations. *Geophysical Research Letters*, *43*(3), 1357–1363. https://doi.org/10.1002/2015gl067392

Hanak, E., & Lund, J. R. (2012). Adapting California's water management to climate change. *Climatic Change*, *111*(1), 17–44. https://doi.org/10.1007/s10584-011-0241-3

Held, I. M., & Soden, B. J. (2006). Robust responses of the hydrological cycle to global warming. *Journal of Climate*, *19*(21), 5686–5699. https://doi.org/10.1175/jcli3990.1

Hennessy, K. J., Gregory, J. M., & Mitchell, J. F. B. (1997). Changes in daily precipitation under enhanced greenhouse conditions. *Climate Dynamics*, *13*(9), 667–680. https://doi.org/10.1007/s003820050189

Hersbach, H., Bell, B., Berrisford, P., Hirahara, S., Horányi, A., Muñoz-Sabater, J., et al. (2020). The ERA5 global reanalysis. *Quarterly Journal of the Royal Meteorological Society*, *146*(730), 1999–2049. https://doi.org/10.1002/qj.3803

Hosseini-Moghari, S.-M., Sun, S., Tang, Q., & Groisman, P. Y. (2022). Scaling of precipitation extremes with temperature in China's mainland: Evaluation of satellite precipitation data. *Journal of Hydrology*, *606*, 127391. https://doi.org/10.1016/j.jhydrol.2021.127391

Huang, X., Swain, D. L., & Hall, A. D. (2020). Future precipitation increase from very high resolution ensemble downscaling of extreme atmospheric river storms in California. *Science Advances*, *6*(29), eaba1323. https://doi.org/10.1126/sciadv.aba1323

Lenderink, G., de Vries, H., Fowler, H. J., Barbero, R., van Ulft, B., & van Meijgaard, E. (2021). Scaling and responses of extreme hourly precipitation in three climate experiments with a convection-permitting model. *Philosophical Transactions of the Royal Society A*, *379*(2195), 20190544. https://doi.org/10.1098/rsta.2019.0544

Lenderink, G., Mok, H. Y., Lee, T. C., & Van Oldenborgh, G. J. (2011). Scaling and trends of hourly precipitation extremes in two different climate zones–Hong Kong and The Netherlands. *Hydrology and Earth System Sciences*, *15*(9), 3033–3041. https://doi.org/10.5194/hess-15-3033-2011

Lenderink, G., & Van Meijgaard, E. (2008). Increase in hourly precipitation extremes beyond expectations from temperature changes. *Nature Geoscience*, *1*(8), 511–514. https://doi.org/10.1038/ngeo262

Lenderink, G., & Van Meijgaard, E. (2010). Linking increases in hourly precipitation extremes to atmospheric temperature and moisture changes. *Environmental Research Letters*, *5*(2), 025208. https://doi.org/10.1088/1748-9326/5/2/025208

Livneh, B., Rosenberg, E. A., Lin, C., Nijssen, B., Mishra, V., Andreadis, K. M., et al. (2013). A long-term hydrologically based dataset of land surface fluxes and states for the conterminous United States: Update and extensions. *Journal of Climate*, *26*(23), 9384–9392. https://doi.org/10.1175/jcli-d-12-00508.1

Loriaux, J. M., Lenderink, G., De Roode, S. R., & Siebesma, A. P. (2013). Understanding convective extreme precipitation scaling using observations and an entraining plume model. *Journal of the Atmospheric Sciences*, *70*(11), 3641–3655. https://doi.org/10.1175/jas-d-12-0317.1

Lott, N., Baldwin, R., & Jones, P. (2001). *The FCC integrated surface hourly database: A new resource of global climate data*. National Climatic Data Center.

Lundquist, J. D., Minder, J. R., Neiman, P. J., & Sukovich, E. (2010). Relationships between barrier jet heights, orographic precipitation gradients, and streamflow in the northern Sierra Nevada. *Journal of Hydrometeorology*, *11*(5), 1141–1156. https://doi.org/10.1175/2010jhm1264.1

Magan, B., Kim, S., Wasko, C., Barbero, R., Moron, V., Nathan, R., & Sharma, A. (2020). Impact of atmospheric circulation on the rainfall-temperature relationship in Australia. *Environmental Research Letters*, *15*(9), 094098. https://doi.org/10.1088/1748-9326/abab35

Mahoney, K., Swales, D., Mueller, M. J., Alexander, M., Hughes, M., & Malloy, K. (2018). An examination of an inland-penetrating atmospheric river flood event under potential future thermodynamic conditions. *Journal of Climate*, *31*(16), 6281–6297. https://doi.org/10.1175/jcli-d-18-0118.1

Martinkova, M., & Kysely, J. (2020). Overview of observed Clausius-Clapeyron scaling of extreme precipitation in midlatitudes. *Atmosphere*, *11*(8), 786. https://doi.org/10.3390/atmos11080786

Masson-Delmotte, V., P. Zhai, A. Pirani, S. L. Connors, C. Péan, S. Berger, et al. (eds.), (2021). *IPCC, 2021: Climate change 2021: The physical science basis. Contribution of working group I to the sixth assessment report of the intergovernmental panel on climate change* (pp. 2391). Cambridge University Press. https://doi.org/10.1017/9781009157896

Michaelis, A. C., Gershunov, A., Weyant, A., Fish, M. A., Shulgina, T., & Ralph, F. M. (2022). Atmospheric river precipitation enhanced by climate change: A case study of the storm that contributed to California's Oroville Dam crisis. *Earth's Future*, *10*(3), e2021EF002537. https://doi.org/10.1029/2021ef002537

Najibi, N. (2023). Extreme precipitation-temperature scaling in California: The role of atmospheric rivers. *Geophysical Research Letters*, *50*, e2023GL104606. https://doi.org/10.5281/zenodo.7390670

Najibi, N., Mukhopadhyay, S., & Steinschneider, S. (2022). Precipitation scaling with temperature in the Northeast US: Variations by weather regime, season, and precipitation intensity. *Geophysical Research Letters*, *49*(8), e2021GL097100. https://doi.org/10.1029/2021gl097100

Nusbaumer, J., & Noone, D. (2018). Numerical evaluation of the modern and future origins of atmospheric river moisture over the West Coast of the United States. *Journal of Geophysical Research: Atmospheres*, *123*(12), 6423–6442. https://doi.org/10.1029/2017jd028081

O'Gorman, P. A., & Schneider, T. (2009a). The physical basis for increases in precipitation extremes in simulations of 21st-century climate change. *Proceedings of the National Academy of Sciences of the United States of America*, *106*(35), 14773–14777. https://doi.org/10.1073/pnas.0907610106

O'Gorman, P. A., & Schneider, T. (2009b). Scaling of precipitation extremes over a wide range of climates simulated with an idealized GCM. *Journal of Climate*, *22*(21), 5676–5685. https://doi.org/10.1175/2009jcli2701.1

Panthou, G., Mailhot, A., Laurence, E., & Talbot, G. (2014). Relationship between surface temperature and extreme rainfalls: A multi-time-scale and event-based analysis. *Journal of Hydrometeorology*, *15*(5), 1999–2011. https://doi.org/10.1175/jhm-d-14-0020.1

Payne, A. E., Demory, M. E., Leung, L. R., Ramos, A. M., Shields, C. A., Rutz, J. J., et al. (2020). Responses and impacts of atmospheric rivers to climate change. *Nature Reviews Earth & Environment*, *1*(3), 143–157. https://doi.org/10.1038/s43017-020-0030-5

Pendergrass, A. G. (2018). What precipitation is extreme? *Science*, *360*(6393), 1072–1073. https://doi.org/10.1126/science.aat1871

Plummer, M. (2003). Jags: A program for analysis of Bayesian graphical models using Gibbs sampling. In *Proceedings of the 3rd international workshop on distributed statistical computing* (Vol. 124).

Polade, S. D., Gershunov, A., Cayan, D. R., Dettinger, M. D., & Pierce, D. W. (2017). Precipitation in a warming world: Assessing projected hydro-climate changes in California and other Mediterranean climate regions. *Scientific Reports*, *7*(1), 1–10. https://doi.org/10.1038/s41598-017-11285-y

Prein, A. F., Rasmussen, R. M., Ikeda, K., Liu, C., Clark, M. P., & Holland, G. J. (2017). The future intensification of hourly precipitation extremes. *Nature Climate Change*, *7*(1), 48–52. https://doi.org/10.1038/nclimate3168

Ralph, F. M., Neiman, P. J., & Rotunno, R. (2005). Dropsonde observations in low-level jets over the northeastern Pacific Ocean from CALJET-1998 and PACJET-2001: Mean vertical-profile and atmospheric-river characteristics. *Monthly Weather Review*, *133*(4), 889–910. https://doi.org/10.1175/mwr2896.1

Ralph, F. M., Neiman, P. J., & Wick, G. A. (2004). Satellite and CALJET aircraft observations of atmospheric rivers over the eastern North Pacific Ocean during the winter of 1997/98. *Monthly Weather Review*, *132*(7), 1721–1745. https://doi.org/10.1175/1520-0493(2004)132<1721:sacaoo>2.0.co;2

Ralph, F. M., Rutz, J. J., Cordeira, J. M., Dettinger, M., Anderson, M., Reynolds, D., et al. (2019). A scale to characterize the strength and impacts of atmospheric rivers. *Bulletin of the American Meteorological Society*, *100*(2), 269–289. https://doi.org/10.1175/bams-d-18-0023.1

Rhoades, A. M., Jones, A. D., Srivastava, A., Huang, H., O'Brien, T. A., Patricola, C. M., et al. (2020). The shifting scales of western US landfalling atmospheric rivers under climate change. *Geophysical Research Letters*, *47*(17), e2020GL089096. https://doi.org/10.1029/2020gl089096

Rutz, J. J., Steenburgh, W. J., & Ralph, F. M. (2014). Climatological characteristics of atmospheric rivers and their inland penetration over the western United States. *Monthly Weather Review*, *142*(2), 905–921. https://doi.org/10.1175/mwr-d-13-00168.1

Seager, R., Naik, N., & Vecchi, G. A. (2010). Thermodynamic and dynamic mechanisms for large-scale changes in the hydrological cycle in response to global warming. *Journal of Climate*, *23*(17), 4651–4668. https://doi.org/10.1175/2010jcli3655.1

Shaw, S. B., Royem, A. A., & Riha, S. J. (2011). The relationship between extreme hourly precipitation and surface temperature in different hydroclimatic regions of the United States. *Journal of Hydrometeorology*, *12*(2), 319–325. https://doi.org/10.1175/2011jhm1364.1

Shields, C. A., & Kiehl, J. T. (2016). Simulating the pineapple express in the half degree community climate system model, CCSM4. *Geophysical Research Letters*, *43*(14), 7767–7773. https://doi.org/10.1002/2016gl069476

Smith, A., Lott, N., & Vose, R. (2011). The integrated surface database: Recent developments and partnerships. *Bulletin of the American Meteorological Society*, *92*(6), 704–708. https://doi.org/10.1175/2011bams3015.1

Smith, B. L., Yuter, S. E., Neiman, P. J., & Kingsmill, D. E. (2010). Water vapor fluxes and orographic precipitation over northern California associated with a landfalling atmospheric river. *Monthly Weather Review*, *138*(1), 74–100. https://doi.org/10.1175/2009mwr2939.1

Steinschneider, S., & Najibi, N. (2022). Observed and projected scaling of daily extreme precipitation with dew point temperature at annual and seasonal scales across the northeastern United States. *Journal of Hydrometeorology*, *23*(3), 403–419.

Sun, X., & Wang, G. (2022). Causes for the negative scaling of extreme precipitation at high temperatures. *Journal of Climate*, *35*(18), 6119–6134. https://doi.org/10.1175/jcli-d-22-0142.1

Swain, D. L., Langenbrunner, B., Neelin, J. D., & Hall, A. (2018). Increasing precipitation volatility in twenty-first-century California. *Nature Climate Change*, *8*(5), 427–433. https://doi.org/10.1038/s41558-018-0140-y

Trenberth, K. E., Dai, A., Rasmussen, R. M., & Parsons, D. B. (2003). The changing character of precipitation. *Bulletin of the American Meteorological Society*, *84*(9), 1205–1218. https://doi.org/10.1175/bams-84-9-1205

Utsumi, N., Seto, S., Kanae, S., Maeda, E. E., & Oki, T. (2011). Does higher surface temperature intensify extreme precipitation? *Geophysical Research Letters*, *38*(16), L16708. https://doi.org/10.1029/2011gl048426

Visser, J. B., Wasko, C., Sharma, A., & Nathan, R. (2020). Resolving inconsistencies in extreme precipitation-temperature sensitivities. *Geophysical Research Letters*, *47*(18), e2020GL089723. https://doi.org/10.1029/2020gl089723

Visser, J. B., Wasko, C., Sharma, A., & Nathan, R. (2021). Eliminating the "hook" in precipitation–temperature scaling. *Journal of Climate*, *34*(23), 9535–9549. https://doi.org/10.1175/jcli-d-21-0292.1

Wang, G., & Sun, X. (2022). Monotonic increase of extreme precipitation intensity with temperature when controlled for saturation deficit. *Geophysical Research Letters*, *49*(7), e2022GL097881. https://doi.org/10.1029/2022gl097881

Warner, M. D., Mass, C. F., & Salathé, E. P. (2015). Changes in winter atmospheric rivers along the North American west coast in CMIP5 climate models. *Journal of Hydrometeorology*, *16*(1), 118–128. https://doi.org/10.1175/jhm-d-14-0080.1

Wasko, C., Lu, W. T., & Mehrotra, R. (2018). Relationship of extreme precipitation, dry-bulb temperature, and dew point temperature across Australia. *Environmental Research Letters*, *13*(7), 074031. https://doi.org/10.1088/1748-9326/aad135

Wasko, C., & Sharma, A. (2014). Quantile regression for investigating scaling of extreme precipitation with temperature. *Water Resources Research*, *50*(4), 3608–3614. https://doi.org/10.1002/2013wr015194

Wasko, C., Sharma, A., & Johnson, F. (2015). Does storm duration modulate the extreme precipitation-temperature scaling relationship? *Geophysical Research Letters*, *42*(20), 8783–8790. https://doi.org/10.1002/2015gl066274

Wu, P., Christidis, N., & Stott, P. (2013). Anthropogenic impact on Earth's hydrological cycle. *Nature Climate Change*, *3*(9), 807–810. https://doi.org/10.1038/nclimate1932

Yu, K., & Moyeed, R. A. (2001). Bayesian quantile regression. *Statistics & Probability Letters*, *54*(4), 437–447. https://doi.org/10.1016/s0167-7152(01)00124-9

Zhang, P., Chen, G., Ma, W., Ming, Y., & Wu, Z. (2021). Robust atmospheric river response to global warming in idealized and comprehensive climate models. *Journal of Climate*, *34*(18), 7717–7734. https://doi.org/10.1175/jcli-d-20-1005.1

Zhang, W., Villarini, G., & Wehner, M. (2019). Contrasting the responses of extreme precipitation to changes in surface air and dew point temperatures. *Climatic Change*, *154*(1–2), 257–271. https://doi.org/10.1007/s10584-019-02415-8

Zhang, X., Zwiers, F. W., Li, G., Wan, H., & Cannon, A. J. (2017). Complexity in estimating past and future extreme short-duration rainfall. *Nature Geoscience*, *10*(4), 255–259. https://doi.org/10.1038/ngeo2911